

Orthorhombic distortion on Li intercalation in anatase

Marina V. Koudriachova and Simon W. de Leeuw

Computational Physics, Department of Applied Physics, TU Delft, Lorentzweg 1, 2628 CJ Delft, The Netherlands

Nicholas M. Harrison

Department of Chemistry, Imperial College of Science, Technology and Medicine, London, SW7 2AY, United Kingdom and CLRC, Daresbury Laboratory, Daresbury, Warrington WA4 4AD, United Kingdom

(Received 19 May 2003; revised manuscript received 1 October 2003; published 19 February 2004)

The mechanism of the tetragonal-to-orthorhombic transformation upon Li-intercalation into anatase structured titania has been studied using first principle calculations. The primary mechanism for the formation of the orthorhombic phase is found to be the accommodation of donated charge in localized Ti- d_{yz} orbitals leading to a cooperative Jahn-Teller-like distortion of the lattice. This model is examined further by considering electron addition states in pure anatase and the analogous structures of $\text{H}_{0.5}\text{TiO}_2$ and $\text{Na}_{0.5}\text{TiO}_2$. It is shown that the rigid band model is not valid and population of the degenerate Ti- $d_{xy,yz}$ orbitals occurs beyond a critical concentration due to the repulsive interaction of the localized electrons. It is shown that the stability of the $\text{Li}_{0.5}\text{TiO}_2$ structure is related to the similarity of the ionic radius of Li^+ and Ti^{+3} ions. Optimal configurations of $\text{H}_{0.5}\text{TiO}_2$ and $\text{Na}_{0.5}\text{TiO}_2$ are also predicted.

DOI: 10.1103/PhysRevB.69.054106

PACS number(s): 61.50.Ah, 64.60.-i, 71.20.-b

I. INTRODUCTION

Anatase-structured TiO_2 is currently being studied for potential applications in solar cells, Li-rechargeable batteries, electrochromic displays, and hydrogen sensors.¹⁻⁵ The flexible electronic structure of the titanium ion allows electrons donated by guest ions to be accommodated while the open structure provides space for the intercalation of cations such as Li^+ , H^+ , and possibly Na^+ . Moreover, titanium dioxide is easily accessible, chemically stable, and cheap; it can also be readily prepared in nanocrystalline form with a high surface area, low density, and low solubility in typical organic electrolytes.

Lithium intercalation into anatase has been studied extensively with a variety of experimental and theoretical techniques.⁵⁻¹³ Electrochemical insertion of Li ions at room temperature proceeds through a two-phase equilibrium of a Li-poor (tetragonal) and a Li-rich (orthorhombic) phase. The latter has the composition $\text{Li}_{0.5}\text{TiO}_2$.^{11,12} The structure of the orthorhombic phase has been clarified in neutron diffraction experiments.¹¹ The mechanism for the orthorhombic distortion has been discussed in terms of approximate crystal orbital calculations and attributed to the formation of Ti-Ti bonds.¹⁴ A chain of Ti-Ti bonds would be expected to enhance electronic conductivity whereas $\text{Li}_{0.5}\text{TiO}_2$ has nonmetallic resistivity.¹¹ Several theoretical studies, mostly Hartree-Fock calculations, have considered the geometry of Li-intercalated anatase but in these studies an orthorhombic distortion of the anatase host was not possible due to constraints imposed on the geometry optimization.¹⁵⁻¹⁷

In a previous study a model of Li intercalation was developed, on the basis of first principles calculations, which correctly predicts that intercalation proceeds as a two phase insertion process as well as reproducing the observed open circuit voltage profile.¹⁸ The current study concerns the structural properties of the lithium rich phase, $\text{Li}_{0.5}\text{TiO}_2$, and the mechanism of the tetragonal-to-orthorhombic phase

transformation. An understanding of this mechanism is important if reliable models of the intercalation behavior of anatase are to be developed. Optimal structures of Na- and H-intercalated anatase are also considered. Significant amounts of H ions are known to be present in anatase, however, to our knowledge, the structure of H-intercalated anatase has not been previously reported.

II. DETAILS OF SIMULATIONS

All calculations were performed using the CASTEP code^{19,20} within the pseudopotential plane-wave formalism and spin polarized density functional theory in the generalized gradient approximation.²¹ Ultrasoft pseudopotentials were used to replace the Ti ($1s, 2s, 2p$) and O ($1s$) core orbitals.²² The k -space sampling was performed on a regular grid with a spacing of 0.1 \AA^{-1} . A plane wave cutoff energy of 380 eV was found to converge the total energy to 0.01 eV per formula unit. Mechanical equilibrium was achieved by unconstrained relaxation of the ionic positions and the size and shape of a computational unit through conjugate-gradient minimization of the total energy to an energy tolerance of 0.02 meV, and forces are reduced to 0.05 eV/\AA .

Atomic and bond populations are estimated using Mulliken population analysis based on atomic orbitals. The absolute populations are dependent on the orbitals chosen but the changes in the charge distribution are reflected reliably.

III. RESULTS AND DISCUSSION

Anatase TiO_2 adopts the tetragonal $I4_1/amd$ space group with cell parameters $a = b = 3.78 \text{ \AA}$ and $c = 9.51 \text{ \AA}$ (Ref. 24) (calculated values $a = b = 3.80 \text{ \AA}$ and $c = 9.51 \text{ \AA}$). The structure consists of distorted TiO_6 octahedra sharing two adjacent edges so that infinite planar double chains are formed (Fig. 1). In the ab planes every O ion has neighboring Ti ions either in the a or the b directions. The soft modes of the

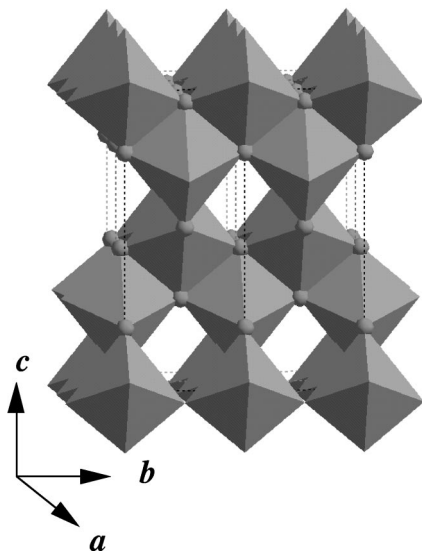


FIG. 1. A polyhedral representation of two primitive unit cells of the anatase structure. In each unit cell there are four vacant octahedral sites between the TiO_6 octahedra.

lattice are uncoupled vibrations in the ab plane and c direction.²⁵ Between the TiO_6 octahedra there are vacant octahedral and tetrahedral sites within which Li ions can be accommodated. It has been established previously that Li insertion proceeds into the octahedral sites.^{11,23} The lower conduction band of anatase consists of $\text{Ti}(d_{xy})$ orbitals. (The Cartesian x , y , and z directions are aligned along the crystallographic a , b , and c directions, respectively.) The degenerate $\text{Ti}(d_{xz,yz})$ are somewhat higher in energy due to local distortions of the TiO_6 octahedra which are in turn due to the edge sharing of the octahedra in the bc and ac planes. The splitting of the t_{2g} orbitals at the bottom of the conduction band is schematically shown in Fig. 2 together with the density of states (DOS) for anatase. The valence band lies between -2.82 eV and -7.65 eV and is predominantly of $\text{O}(2p)$ character while the lower conduction band at -0.8 eV is made up of $\text{Ti}(3d)$ derived states. The computed valence bandwidth of 4.83 eV is comparable to that measured in x-ray photoelectron spectroscopy (XPS) of 4.75 eV.²⁹ The band gap of pure anatase is computed to be ≈ 2 eV while the observed value is approximately 3.2 eV.³⁰ This discrepancy is due to the well known tendency of DFT eigenvalues to underestimate the magnitude of the band gap.

A. The driving mechanism for the orthorhombic distortion

The unit cell of $\text{Li}_{0.5}\text{TiO}_2$ contains two Li ions that can be distributed over the four available octahedral positions in two symmetry inequivalent ways as illustrated in Fig. 3, A and B. Full relaxation of both structures has been performed and in each case leads to an orthorhombic distortion of the lattice. The structure with neighboring octahedra filled (Fig. 3, A) has $Pmma$ symmetry while the structure with the second neighboring octahedra filled (Fig. 3, B) is of $Imm2$ symmetry. The total energy difference between the structures is very small (0.001 eV per formula unit) thus at room tempera-

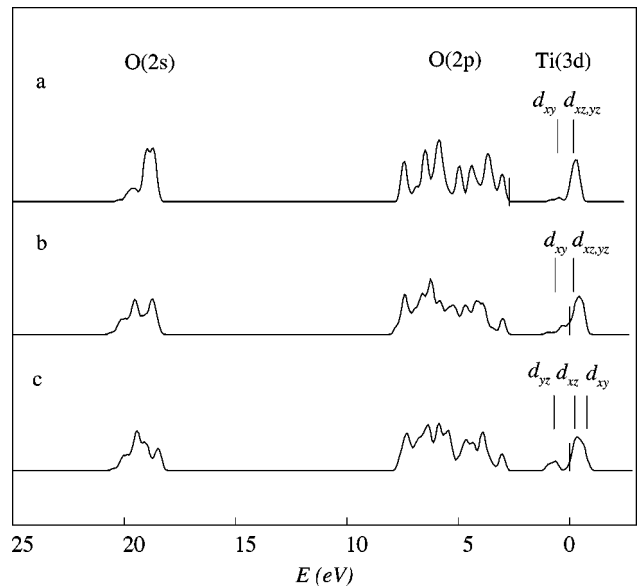


FIG. 2. The density of states for anatase TiO_2 (a), an hypothetical tetragonal $\text{Li}_{0.5}\text{TiO}_2$ structure (b) and the orthorhombic $\text{Li}_{0.5}\text{TiO}_2$ phase (c). The data for the different structures are aligned at the valence band maximum. The Fermi level for each structure is indicated by a vertical line.

ture a random distribution of Li ions over the octahedral sites is expected. The random distribution of Li ions is also apparent in neutron diffraction data.¹¹ In what follows the random distribution is mimicked by averaging structural parameters over the A and B structures resulting in a system with orthorhombic $Imma$ symmetry. The computed geometry of

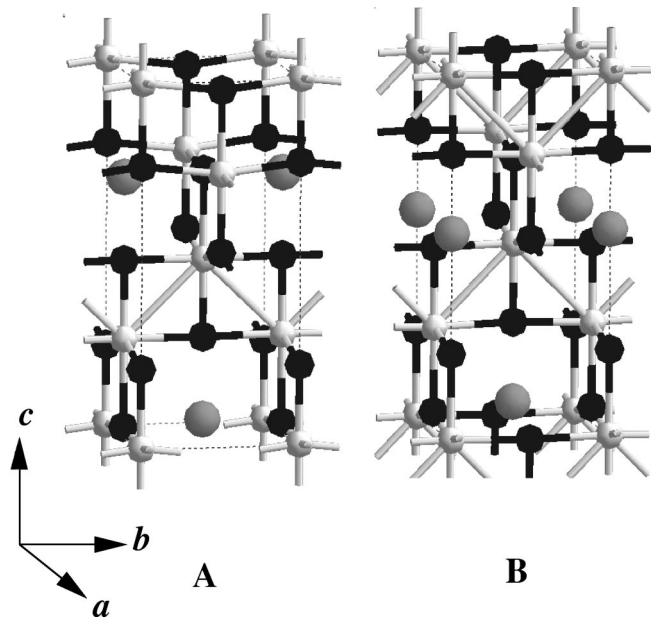


FIG. 3. The primitive unit cells of the two predicted structures with composition $\text{Li}_{0.5}\text{TiO}_2$. In structure A neighboring octahedral sites are occupied while in structure B second neighbor sites are occupied. Ti ions are shown in white, O ions in black, and intercalated cations (and their periodic images) in gray. The orientation of the unit cells is the same as that of bulk anatase in Fig. 1.

TABLE I. Cell parameters of $C_{0.5}\text{TiO}_2$, $C = \text{Li, Na, H, \AA}$.

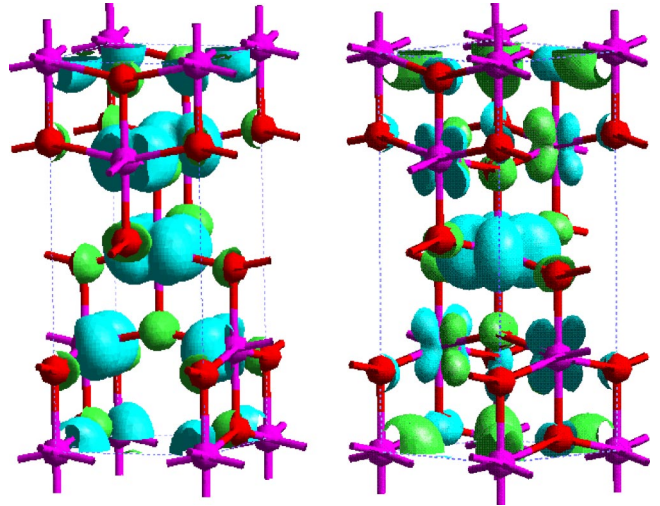
Cation	Structure	a	b	c	Space group
Li	Expt. (Ref. 11)	3.81	4.08	9.05	$Imma$
Li	Expt. (Ref. 12)	3.85	4.06	8.95	$Imma$
Li	A	3.89	3.99	9.02	$Pmma$
Li	B	3.82	4.04	9.08	$Imm2$
Li	Average	3.85	4.02	9.05	$Imma$
Li	C	3.96	3.96	8.85	$P-4m2$
Na		3.38	4.01	12.84	$Pmn21$
H	D	3.85	3.98	9.49	$P-1$
H	E	3.85	3.98	8.99	$Imm2$

$\text{Li}_{0.5}\text{TiO}_2$ is compared to that deduced from diffraction data in Tables I and II. There is excellent agreement between the computed and measured structures. The orthorhombic $\text{Li}_{0.5}\text{TiO}_2$ structure is formed from pure anatase by anisotropic expansion in the ab planes (by 1% in the a direction and 8% in the b direction) and a contraction along the c direction (by 5%). Within this structure the Li ions reside in off-center positions displaced from the center of the octahedral vacancies by $0.035c$ along the c direction. In this position Li ions are fivefold coordinated with Li-O distances ranging from 1.97 to 2.05 Å. These values are close to the Li-O distance of 1.996 Å observed in Li_2O .²⁶

The orthorhombic distortion of the lattice is due to the strong coupling between the orbital occupancy on the Ti sites and the local deformations of the lattice. Within the ionic model each Li is expected to donate an electron to the lattice. At low insertion concentrations the Li-occupied octahedral site expands in the a and b directions equally as the d_{xy} states of the lower anatase conduction band are populated. In principle these orbitals could accommodate all of the donated electrons up to LiTiO_2 and thus one might expect the $\text{Li}_{0.5}\text{TiO}_2$ to expand in the ab plane and to retain tetragonal symmetry. However, this “rigid-band” picture ignores the localisation of the d orbitals and the resultant strong interactions between the occupied states. The effects of these interactions can best be illustrated by a model calculation in which electrons are added to the anatase unit cell (Ti_4O_8) and compensated by a homogeneous positive background charge. A single extra electron is accommodated in the d_{xy} orbitals but addition of a second electron results in alternating ab planes in which d_{xy} and also $d_{xz,yz}$ orbitals are populated. Electrons move into the $d_{xz,yz}$ orbitals due to repulsive

TABLE II. Experimental and calculated internal coordinates in $\text{Li}_{0.5}\text{TiO}_2$.

Atom	Experiment (Ref. 11)			Theory		
	x	y	z	x	y	z
Ti	0.00	0.25	0.887	0	0.25	0.876
O1	0.00	0.25	0.103	0	0.25	0.100
O2	0.00	0.25	0.652	0	0.25	0.649
Li	0.00	0.25	0.343	0	0.25	0.338

FIG. 4. (Color online) Isovalue surfaces of the spin density for anatase doped with one (left panel) and two (right panel) electrons drawn for $S_z = 0.03 \mu_B$.

interactions between electrons in the d_{xy} states. The resultant spin density is displayed in Fig. 4. This strongly suggests that as Li is intercalated into the lattice a critical concentration will be reached at which the degenerate $d_{xz,yz}$ orbitals are populated.

The population analysis of $\text{Li}_{0.5}\text{TiO}_2$ indicates that each Li ion donates $0.86 |e|$ to the lattice (equivalent to $1.7 |e|$ per anatase unit cell) and the system spontaneously distorts to the orthorhombic structure. As a result of the distortion the degeneracy of the d_{xz} and d_{yz} orbitals is lifted as shown in Fig. 2(c). The splittings at the bottom of the conduction band described above are specific to the anatase structure. In rutile the local symmetry of the Ti sites is different and orthorhombic distortion does not occur upon Li intercalation. In rutile the TiO_6 octahedra share edges in the c direction and corners in the ab planes. The distortion of the TiO_6 octahedra induced by such packing lifts the degeneracy of $d_{xz,yz}$ orbitals in pure rutile. The bottom of the conduction band of rutile consist of d_{yz} orbitals which are populated upon Li intercalation.

The role of the distortion can be analyzed by comparing the DOS of the anatase host, the relaxed orthorhombic structure and an hypothetical tetragonal structure, which are displayed in Fig. 2. The latter structure was generated by relaxing lithiated anatase at a Li to Ti ratio of 1/2 under the constraint of tetragonal symmetry. In the tetragonal structure donated charge is accommodated by the $d_{xy,xz,yz}$ states at the bottom of the conduction band, resulting in a metallic ground state with a high DOS at the Fermi level. The major effect of orthorhombic distortion is to split these states and reduce the DOS at the Fermi level. Thus the distortion can be considered as a Peierls, or a cooperative Jahn-Teller-like, distortion of the lattice. In the fully relaxed orthorhombic structure the occupied orbitals are almost purely d_{yz} in character. These states split slightly from the conduction band and form gap states at 1.74 eV above the valence band edge with a width

of 1.5 eV (Fig. 2). Such gap states have been observed previously in the spectroscopy of Li-intercalated rutile, reduced TiO_2 and its surfaces.^{23,31,32}

B. Limitations of the extent of the orthorhombic distortion

The orthorhombic distortion increases the Ti-O distances along b from 1.93 Å to 2.02 Å, which is typical of the Ti^{+3} -O distances observed in Ti_2O_3 (2.02 Å).^{27,28} In the a direction the Ti-O distance increases very slightly from 1.93 Å to 1.95 Å. In essence the additional charge received by the reduced Ti ions localizes in the d_{yz} orbital and the Ti ions adopt Ti-O distances typical for Ti^{+3} ions in the b direction and typical for Ti^{+4} ions in the a direction. The expansion of the lattice along b results in almost colinear Ti-O-Ti contacts in the b direction (Fig. 3). As the typical Li^+ -O and Ti^{+3} -O distances are very similar the expansion in the b direction creates an ideal off-center position for the accommodation of Li^+ ions which also form nearly colinear Li-O-Li contacts along b (Fig. 3). In this off-center position the Li ions are fivefold coordinated to O (Fig. 3). Further expansion of the lattice along the b direction involves stretching the Ti-O and Li-O contacts beyond typical distances and is energetically unfavorable. This limits the extent of the orthorhombic distortion.

The large expansion of the lattice in the b direction is accompanied by a contraction along c . It is important to note that this contraction is not due to a change in the “height” of the octahedra along c (which actually increases slightly) but due to a change in their packing. From the point of view of a layer of octahedra in an ab plane, their expansion allows the layer above to penetrate more deeply. This results in Ti ions adopting off-center positions within the octahedra with Ti-O distances of 2.15 and 1.94 Å along c . The average of these distances is 2.06 Å which is a typical bond length for Ti^{+3} ions in the Ti_2O_3 structure. These asymmetric distortions of the TiO_6 octahedra are reminiscent of the displacements involved in the excitation of the ν_4 and ν_9 vibrational modes at 399 and 507 cm^{-1} .²⁵ These modes have relatively high frequencies but are the softest modes which involve displacements in the c direction and are thus natural distortions of the lattice as it accommodates the contraction of c .

The overall distortion of the structure induces Ti-Ti close contacts of 2.82 Å. The contacts form zigzag “bonded” chains within edge-sharing octahedra exclusively along the b axis. The Ti-Ti contacts are depicted as bonds in Fig. 3. As noted above, the formation of such Ti-Ti bonds has been suggested as a mechanism for the orthorhombic distortion.^{11,14} However, Mulliken analysis of the charge density indicates that there is no significant population of the Ti-Ti close contacts. The Ti-Ti bonding hypothesis can be examined further by considering the behavior of the hypothetical tetragonal structure (Table I, structure C). In this structure close Ti-Ti contacts of 2.91 Å occur and, as in the orthorhombic structure, there is a strong contraction in the c direction. It is clear that the Ti-Ti contacts are induced by the deformations upon Li intercalation and are not a primary cause of the orthorhombic distortion.

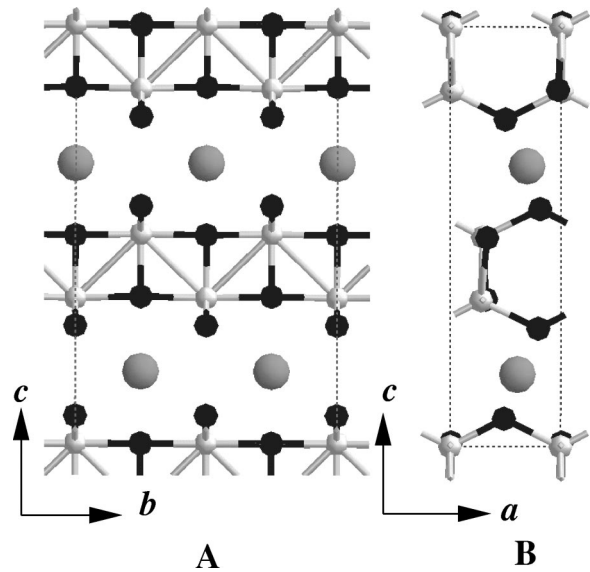


FIG. 5. The predicted structure of $\text{Na}_{0.5}\text{TiO}_2$ viewed along the crystallographic a (A) and b (B) directions.

There are small changes in the valence bandwidth on Li insertion (Fig. 2). More significant changes occur in the semicore level peaks which may be observable in XPS measurements. The $\text{Ti}(3s)$ and $\text{Ti}(3p)$ peaks split by 0.1 and 0.13 eV, respectively, and the bandwidth of the $\text{O}(2s)$ band increases from 1.97 eV to 2.35 eV. These changes reflect the induced structural inequality of the ions and the inhomogeneous distribution of the charge donated by the Li ions.

C. Intercalation of hydrogen and sodium ions

It has been noted above that the similar size of the Li^+ and Ti^{+3} ions plays an important role in the accommodation of lithium ions by the lattice. In order to investigate the influence of the size of the cation on the structure of intercalated anatase additional calculations were performed in which the Li ions were replaced by Na and H ions, and the structure fully relaxed. The resultant optimal configurations of $\text{Na}_{0.5}\text{TiO}_2$ and $\text{H}_{0.5}\text{TiO}_2$ are shown in Figs. 5 and 6, respectively. The calculated cell parameters of the $\text{Na}_{0.5}\text{TiO}_2$ and $\text{H}_{0.5}\text{TiO}_2$ structures are compared to those of $\text{Li}_{0.5}\text{TiO}_2$ in Table I. It is clear that the deformations of the anatase host depend strongly on which cation is intercalated.

To form the layered $\text{Na}_{0.5}\text{TiO}_2$ structure from the $\text{Li}_{0.5}\text{TiO}_2$ structure major distortions of the lattice are required. The c -lattice constant increases by 42% leading to TiO_2 layers along the c direction that are offset in the a direction relative to the analogous layers in the lithiated structure. Between these layers there are only two available octahedral sites and these are fully occupied by Na ions. The Na ions in these positions adopt sixfold coordination to O ions in strongly distorted octahedra. Constrained optimization of the Na structure, in which it is forced to retain the orthorhombic symmetry of the lithiated structure, results in Ti-O bond lengths of 2.1 Å along the b axis, which are significantly longer than those observed in typical Ti^{+3} -O structures (2.02 Å). It appears that the larger Na ion cannot be

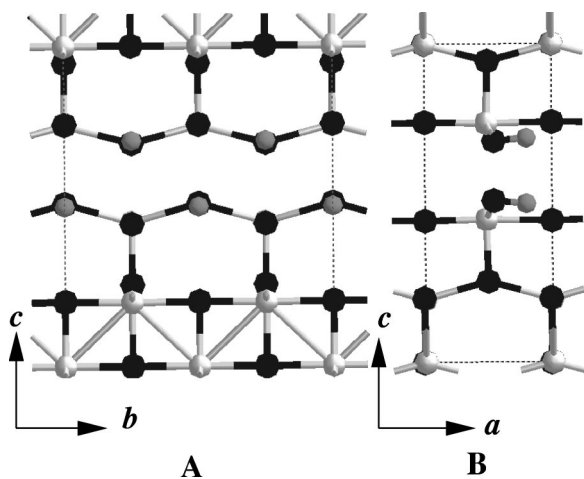


FIG. 6. The predicted structure of $\text{H}_{0.5}\text{TiO}_2$ viewed along the crystallographic a (A) and b (B) directions.

accommodated in an anatase-type structure. The transformation to the layered structure allows Ti-O distances in the a and b directions to be preserved.

$\text{H}_{0.5}\text{TiO}_2$ is stable in the orthorhombic lithiated structure but significant differences in the local geometry occur. The H ion does not sit in the center of an octahedron but forms an hydroxyl group with a bond length of 0.98 Å. Each O-H bond is oriented parallel to a Ti-O bond along either the a or b directions (Fig. 6). While Li and Na ions transfer most of their valence electron density to the lattice (86% and 95%, respectively) the more electronegative H ions donate only 32%. Of this charge 35% is localized on the O ions forming a chemical bond with the H ions and 65% is transferred to the neighboring Ti ions. These O ions have a charge of $-0.78|e|$ whereas O ions receiving charge on Li and Na insertion have a charge of $-0.72|e|$. The formation of an hydroxyl group is reflected in the DOS as a splitting at the bottom of the valence O-2s and O-2p bands as shown in Fig. 7.

The DOS at the Fermi level for both $\text{H}_{0.5}\text{TiO}_2$ and $\text{Na}_{0.5}\text{TiO}_2$ is reduced due to the structural deformations discussed above. Despite the difference in the local geometry of the intercalation site the overall orthorhombic distortion of the lattice is similar to that observed in the lithiated structure. This is entirely consistent with the mechanism for the orthorhombic distortion discussed above. The distortion is due to the accommodation of donated charge by the Ti ions and is thus independent of the local interactions between intercalated cations and of Ti-Ti bond formation. $\text{H}_{0.5}\text{TiO}_2$ hardly contracts in the c direction. This appears to be due to the change of the nature of the O ions forming the O-H bonds

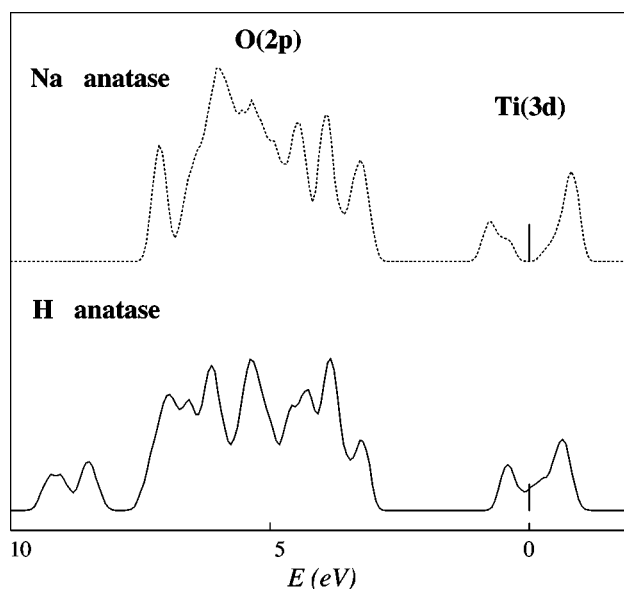


FIG. 7. The density of states for $\text{Na}_{0.5}\text{TiO}_2$ (upper panel, dashed line) and $\text{H}_{0.5}\text{TiO}_2$ (lower panel, solid line). The Fermi level for each structure is indicated by a vertical line.

which are only weakly bonded to the rest of the lattice. In a metastable structure containing O-H groups constrained to be parallel to the c direction this effect is much less pronounced and the structure contacts strongly along the c direction (Table I, structure E).

IV. CONCLUSIONS

The mechanism for the tetragonal-to-orthorhombic transformation upon Li intercalation into anatase TiO_2 has been studied using first principles calculations. It has been demonstrated that the rigid band model does not give a correct picture of the localization of electron density donated on Li intercalation. The formation of the orthorhombic phase is due to the accommodation of donated charge in localized Ti- d orbitals with the occupation of degenerate orbitals above a critical intercalation concentration resulting in a cooperative Jahn-Teller-like distortion of the lattice. It has also been shown that stability of the $\text{Li}_{0.5}\text{TiO}_2$ depends on the similarity of the ionic radius of Li^+ and Ti^{+3} ions. An analogous Na-intercalated anatase structure is unstable with respect to a layered geometry while the H-intercalated structure has significant differences in the geometry of the intercalation site. Structures for $\text{H}_{0.5}\text{TiO}_2$ and $\text{Na}_{0.5}\text{TiO}_2$ are predicted.

¹H. O. Finklea, in *Semiconductor Electrodes, Studies in Physical and Theoretical Chemistry* (Elsevier, Amsterdam, 1988), Vol. 55, pp. 43–145.

²D. O'Hare, in *Inorganic Materials*, edited by D. W. Bruce and D. O'Hare (Wiley, London, 1996), pp. 171–254.

³S. Huang, L. Kavan, A. Kay, and M. Grätzel, *J. Electrochem. Soc.* **141**, 142 (1995).

⁴L. Kavan, M. Grätzel, S. E. Gilbert, C. Klemenz, and H. J. Scheel, *J. Am. Chem. Soc.* **118**, 6716 (1996).

⁵T. Ohzuku, Z. Takehara, and S. Yoshizawa, *Electrochim. Acta* **27**,

- 1263 (1982).
- ⁶M. Voinov, *Proc. Electrochem. Soc.* **81**, 352 (1981).
- ⁷F. Bonino, L. Busani, M. Manstretta, B. Rivolta, and B. Scrosatti, *J. Power Sources* **14**, 261 (1985).
- ⁸B. Zachau-Christiansen, K. West, T. Jacobsen, and S. Atlung, *Solid State Ionics* **28–30**, 1176 (1988).
- ⁹P. Krtíl, D. Fattakhova, L. Kavan, S. Burnside, and M. Grätzel, *Solid State Ionics* **135**, 101 (2000).
- ¹⁰W. J. Macklin and R. J. Neat, *Solid State Ionics* **53–56**, 694 (1992).
- ¹¹R. J. Cava, A. Santoro, D. W. Murphy, S. M. Zahurak, and R. S. Roth, *J. Solid State Chem.* **83**, 64 (1984).
- ¹²R. van de Krol, A. Goossens, and E. A. Meulenkaamp, *J. Electrochem. Soc.* **146**, 3150 (1999).
- ¹³L. Kavan, J. Rathouský, M. Grätzel, V. Shklover, and A. Zukal, *J. Phys. Chem. B* **104**, 12 012 (2000).
- ¹⁴G. Nuspl, K. Yoshizawa, and T. Yamabe, *J. Mater. Chem.* **7**, 2529 (1997).
- ¹⁵A. Stashans, S. Lunell, R. Begstrom, A. Hagfeldt, and S. E. Lindquist, *Phys. Rev. B* **53**, 159 (1996).
- ¹⁶S. Lunell, A. Stashans, L. Ojamäe, H. Lindström, and A. Hagfeldt, *J. Am. Chem. Soc.* **119**, 7374 (1997).
- ¹⁷W. C. Mackrodt, *J. Solid State Chem.* **142**, 428 (1999).
- ¹⁸M. V. Koudriachova, N. M. Harrison, and S. W. de Leeuw, *Phys. Rev. Lett.* **86**, 1275 (2001).
- ¹⁹M. C. Payne, M. P. Teter, D. C. Allan, T. A. Arias, and J. D. Joannopoulos, *Rev. Mod. Phys.* **64**, 1045 (1992).
- ²⁰CASTEP 3.9 Academic version, licensed under the UKCP-MSI agreement, 1999.
- ²¹J. P. Perdew, *Phys. Rev. B* **34**, 7406(E) (1986).
- ²²D. Vanderbilt, *Phys. Rev. B* **41**, 7892 (1990).
- ²³M. V. Koudriachova, N. M. Harrison, and S. W. de Leeuw, *Phys. Rev. B* **65**, 235423 (2002).
- ²⁴J. K. Burdet, T. Hughbanks, G. J. Miller, J. W. Richardson, and J. V. Smith, *J. Am. Chem. Soc.* **109**, 3639 (1987).
- ²⁵T. Ohsaka, F. Izumi, and Y. Fujiki, *J. Raman Spectrosc.* **7**, 321 (1978).
- ²⁶J. M. Bijvoet, A. Claassen, and A. Karssen, *Proc. K. Ned. Akad. Wet.* **29**, 1286 (1926).
- ²⁷R. E. Newnham and Y. M. de Haan, *Z. Kristallographie, Kristallgeometrie, Kristallphysik, Kristallchemie* **117**, 235 (1962).
- ²⁸G. Shirane, S. J. Pickarty, and R. Newnham, *J. Phys. Chem. Solids* **12**, 155 (1960).
- ²⁹R. Sanjinès, H. Tang, H. Berger, F. Gozzo, G. Margaritondo, and F. Levy, *J. Appl. Phys.* **75**, 2045 (1994).
- ³⁰H. Tang, F. Levy, H. Berger, and P. E. Schmid, *Phys. Rev. B* **52**, 7771 (1995).
- ³¹J. Muscat, N. M. Harrison, and G. Thornton, *Phys. Rev. B* **59**, 15 457 (1999).
- ³²A. T. Paxton and L. Thiên-Nga, *Phys. Rev. B* **57**, 1579 (1998).